Supporting Information

Polymerization-induced fluoroacetonitrile-based heterogeneous lithium metal batteries

Experiment

Preparation of Oleophilic Garnet (LLZO) Nanoparticles. Oleophilic garnet nanoparticles were synthesized according to a modified procedure from our previous work.[1] $Li_{6.5}La_3Zr_{1.5}Ta_{0.5}O_{12}$ (LLZO) was prepared via a solid-state method. Stoichiometric amounts of raw materials ($LiOH{\cdot}H_2O$, $La(OH)_3$, ZrO_2, Ta_2O_5) were ball-milled in ethanol at 400 rpm for 12 h, sequentially calcined at 900 ^oC for 12 h and 1150 ^oC for 10 min, and then ball-milled again for 12 h to obtain the final LLZO powder. Subsequently, the as-prepared LLZO was treated with a 1 M HCl solution and trimethylsilyl trifluoromethanesulfonate to remove the surface Li_2CO_3 layer. The conditioned LLZO was then dispersed in a precursor solution containing 1H,1H,2H,2H-perfluorooctyl trichlorosilane (PFOTS, 0.1 mL), n-Hexane (5 mL), followed by stirring for 30 min. The final oleophilic LLZO nanoparticles were collected by curing at 60 ^oC for 0.5 h and 110 ^oC for 1 h, and stored in Ar-filled glovebox.

Preparation of Trilayer Separator. The trilayer separator was fabricated according to our previous method.[2] First, the PVDF-HFP precursor solution was prepared by dissolving 0.6 g of poly(vinylidene fluoride-co-hexafluoropropylene (PVDF-HFP, Kynar Flex 2801) in a mixture of acetone and deionized water (10:1 v/v). The solution was stirred at 60 °C for 20 min and then continuously stirred at room temperature for 6 h. Subsequently, the PVDF-HFP/LLZO precursor was prepared by mixing 1.76 g of oleophilic LLZO nanoparticles, 0.24 g of PVDF-HFP, and 0.2 g of LiTFSI in 9 mL of N,N-dimethylformamide (DMF). The trilayer separator was then assembled via a tape-casting process. The PVDF-HFP/LLZO precursor was first cast onto a commercial PE

membrane using a doctor blade with a 40 μm gap. This layer was vacuum-dried at 60 ^{o}C for 2 h to remove residual solvent. Next, the PVDF-HFP precursor was applied as a second layer over the dried PVDF-HFP/LLZO layer, again using the doctor blade. The resulting composite structure was finally vacuum-dried at 60 °C for 24 h to ensure complete solvent removal and enhance interlayer adhesion.

Preparation of FAN-based Electrolyte. The polymer precursor was prepared by mixing trifluoroethyl acrylate (TFEA) with poly(ethylene glycol) diacrylate (PEGDA, 1 mol%) as a cross-linker and azobisisobutyronitrile (AIBN, 1 mol%) as a thermal initiator. Separately, a 1.3 M LiFSI in fluoroacetonitrile (FAN) solvent was prepared as the liquid electrolyte. The FAN-based liquid electrolyte was then mixed with the polymer precursor at a 9:1 weight ratio. The mixture was kept at 60 °C overnight to complete the thermally activated crosslinking polymerization, yielding the final FAN-based polymerization electrolyte.

Structural Characterization. The morphologies and chemical compositions of the cycled electrodes were analyzed using scanning electron microscopy (SEM, JEOL JSM-7800F) and X-ray photoelectron spectroscopy (XPS, Axis Ultra DLD, Shimadzu). To prevent air exposure, the cycled Li metal electrodes were transferred from an Ar-filled glovebox to the spectrometer using a dedicated, airtight transfer vessel. The thermal stability was evaluated using a thermogravimetric test (Netzsch TG209) in Ar atmosphere from room temperature to 200 ^{o}C at a scan rate of 10 ^{o}C min^{-1}.

Physical Characterization. The porosity of the as-prepared trilayer and pristine PE separators was determined by immersing them in n-butanol for 2 hours and then

calculating the value using Eq. (1):[3]

$$P = \frac{m - m_0}{\rho V} \times 100\% \quad (1)$$

where m_0 and m are the weights of the separators before and after n-butanol absorption, respectively; ρ is the density of n-butanol; and V is the separator volume calculated from its thickness and diameter. To measure electrolyte uptake stability, the separators were immersed in a 1.3 M LiFSI-fluoroacetonitrile (FAN) electrolyte for 2 hours. The surface electrolyte was then blotted with filter paper before weighing. The electrolyte uptake (η) was calculated using Eq. (2):

$$\eta = \frac{w - w_0}{w_0} \times 100\% \quad (2)$$

where w_0 and w are the weights of pristine and swollen separators.

Electrochemical Measurements. Ionic conductivity was evaluated by electrochemical impedance spectroscopy (EIS) over a temperature range of -70 °C to 60 °C using an Autolab 302N station. The measurements were performed over a frequency range of 1 MHz to 1.0 Hz. The measurement cell consisted of two parallel copper plates with a spacer, which served as blocking electrodes and were immersed just below the electrolyte level without applying external pressure. The ionic conductivity (σ) was calculated using Eq. (3):

$$\sigma = \frac{1}{R} \cdot \frac{L}{S} \quad (3)$$

where L is the thickness of the electrolyte, R is the bulk resistance derived from the impedance spectrum, and A is the contact area between the electrolyte and the blocking electrodes. The electrolyte thickness (L) equates to the spacer thickness between the Cu

electrodes, measured as 0.40 ± 0.04 cm. All EIS measurements were performed after stabilizing the samples at each temperature for 1 hour. The temperature-dependent conductivity of the FAN-based electrolytes was fitted using the Vogel–Fulcher–Tammann (VFT) equation:[4]

$$\sigma = A' exp\left(-\frac{B}{R(T - T_0)}\right) \quad (4)$$

where B, A', R, T_0, *and* T are VFT pseudo-activation energy, pre-exponential factor, gas constant, equilibrium glass transition temperature, and absolute temperature, respectively.

Cyclic voltammetry (CV) measurements were performed using an Autolab electrochemical workstation. Li|Al cells were assembled with a trilayer separator in an asymmetric electrolyte configuration: the FAN-based electrolyte was in contact with the aluminum working electrode, while the ether-based electrolyte (1 M LiTFSI and 2 wt.% $LiNO_3$ in DOL/DME) faced the lithium metal counter/reference electrode. For comparison, control cells were assembled using only the single ether-based electrolyte. All cells were scanned at a rate of 1 mV s^{-1} over a voltage range of 2.8 to 4.5 V versus Li^+/Li.

Heterogeneous lithium metal batteries (half cells) were assembled with CR2016 coin cells with a stack pressure of 50 kg cm^{-2}, using the FAN-based electrolyte (25 μL) facing the cathode and an ether electrolyte (1 M LiTFSI and 2 wt.% $LiNO_3$ in DOL/DME, 25 μL) facing the Li metal anode (0.4 mm diameter and 10 mm thickness). The NCM811 cathode was fabricated by mixing the active material, conductive carbon, and poly(vinylidene fluoride) binder at a weight ratio of 8:1:1 in N-methyl-2-

pyrrolidone (NMP) and then coating the slurry onto an aluminum foil. The mass loading of the active material was approximately 2 mg cm^{-2}. Galvanostatic charge and discharge tests were carried out in a voltage window of 2.8 to 4.3 V (vs. Li^+/Li) under constant current mode.

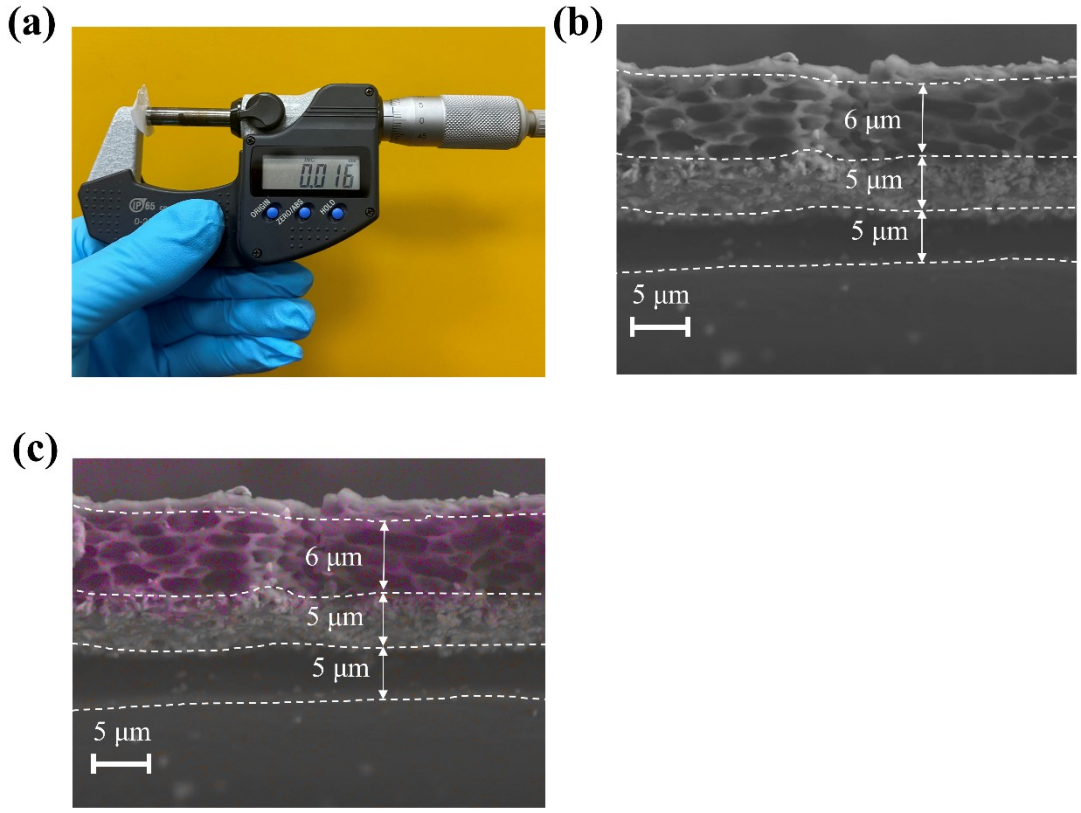

Figure S1. (a) Digital photograph, (b) side-view SEM image, (c) side-view fluorine EDS mapping of trilayer separator.

To assess the effectiveness of the trilayer architecture in blocking FAN electrolyte permeation, a tracer experiment was designed. First, 50 µL of the FAN-based electrolyte—comprising 1.3 M LiFSI in FAN mixed with a TFEA-based solution at a 9:1 weight ratio—was added into the porous PVDF-HFP layer of the trilayer separator (16 mm diameter), followed by thermally activated polymerization. Subsequently, 50 µL of a 1:1 (v/v) mixture of DOL and DME solvents was added into the porous PE layer of the same separator. The assembly was then set aside for 36 hours to allow saturation of the respective layers with the FAN and DOL/DME electrolytes.

After this equilibration period, energy-dispersive X-ray spectroscopy (EDS) mapping was performed to track the distribution of fluorine (F). Fluorine serves as an

effective tracer in this system, as it is a major constituent of the FAN-based electrolyte (FAN solvent, LiFSI salt, and TFEA additive) but is absent from the DOL/DME solvent mixture. This protocol enables a straightforward evaluation of the trilayer architecture's ability to block crossover of the FAN electrolyte from one compartment to the other.

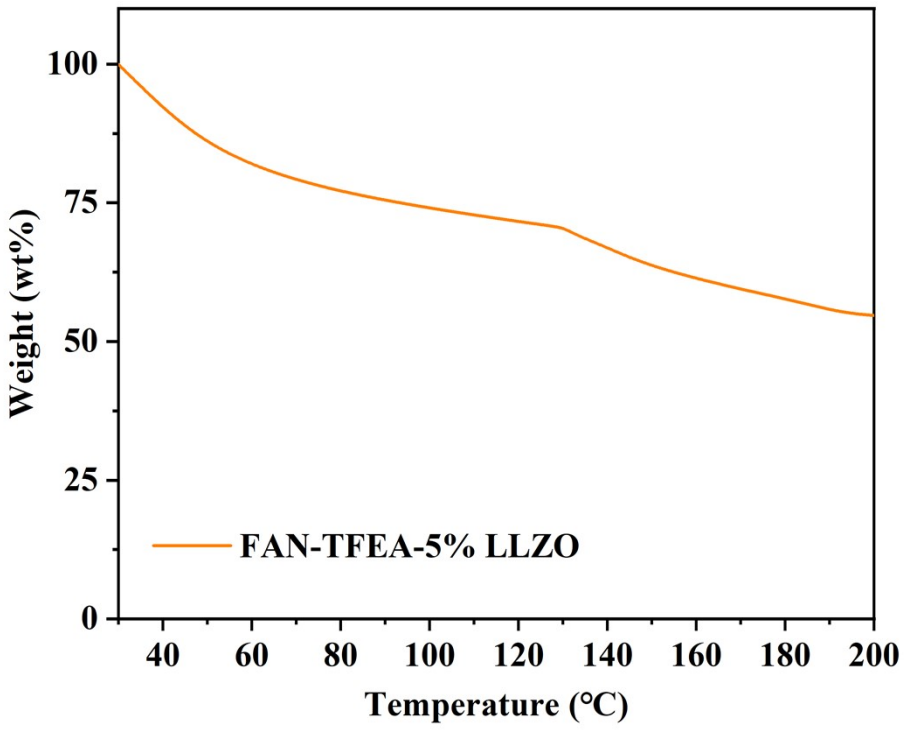

Figure S2. Thermogravimetric curve of FAN-TFEA-5% LLZO electrolyte.

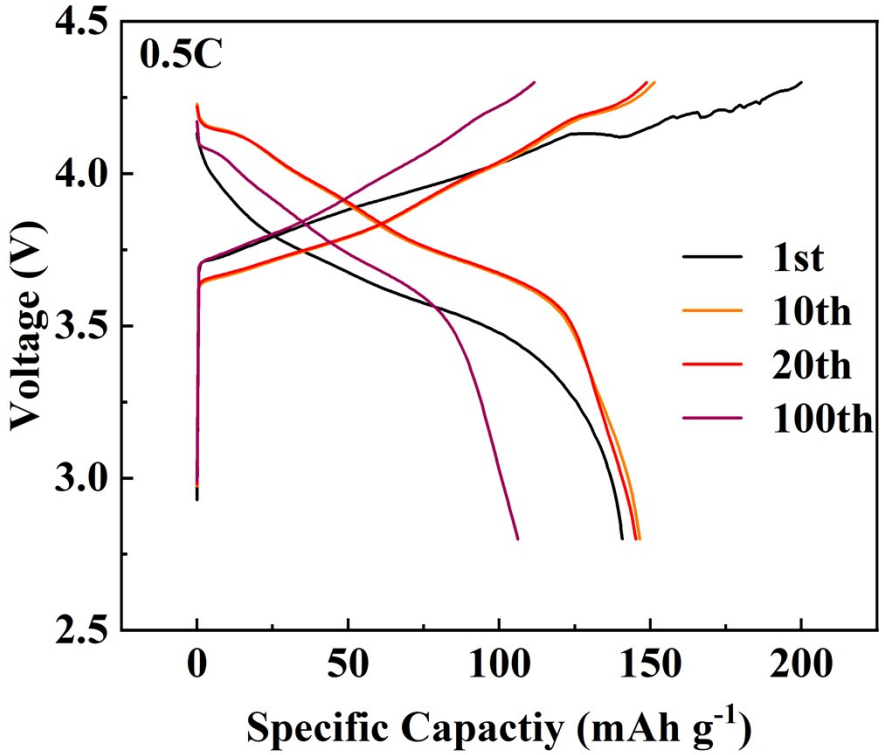

Figure S3. Voltage−capacity profiles of LMB with heterogeneous FAN-TFEA-5% LLZO electrolyte at 0.5 C.

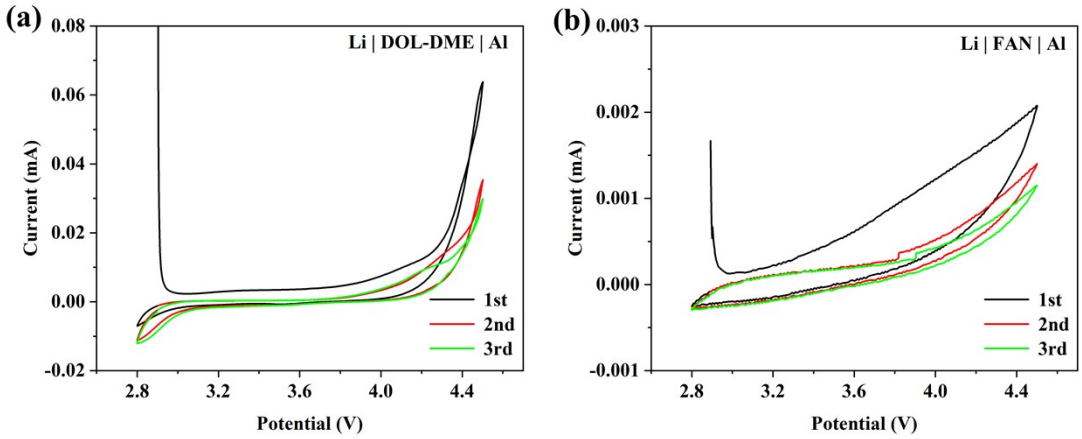

Figure S4. CV curves of Li|Al cells using (a) single DOL-DME-based ether electrolyte (b) FAN-TFEA-5% LLZO electrolyte.

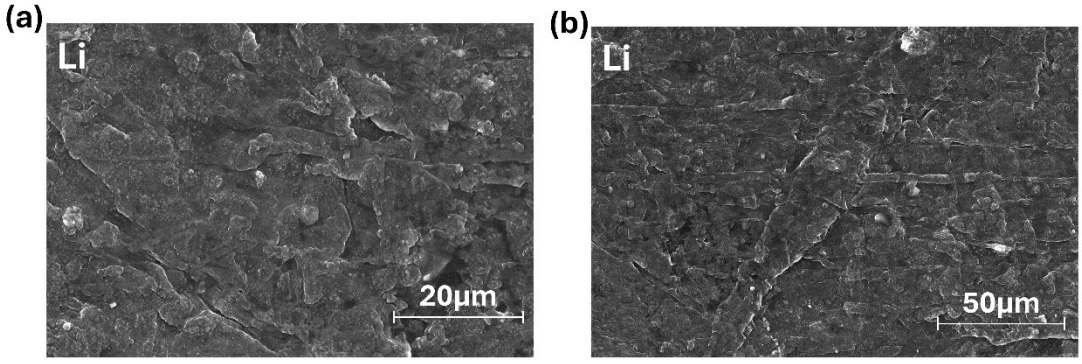

Figure S5. SEM images of Li metal anodes after 10 cycles in LMBs with FAN-TFEA-5% LLZO electrolyte.

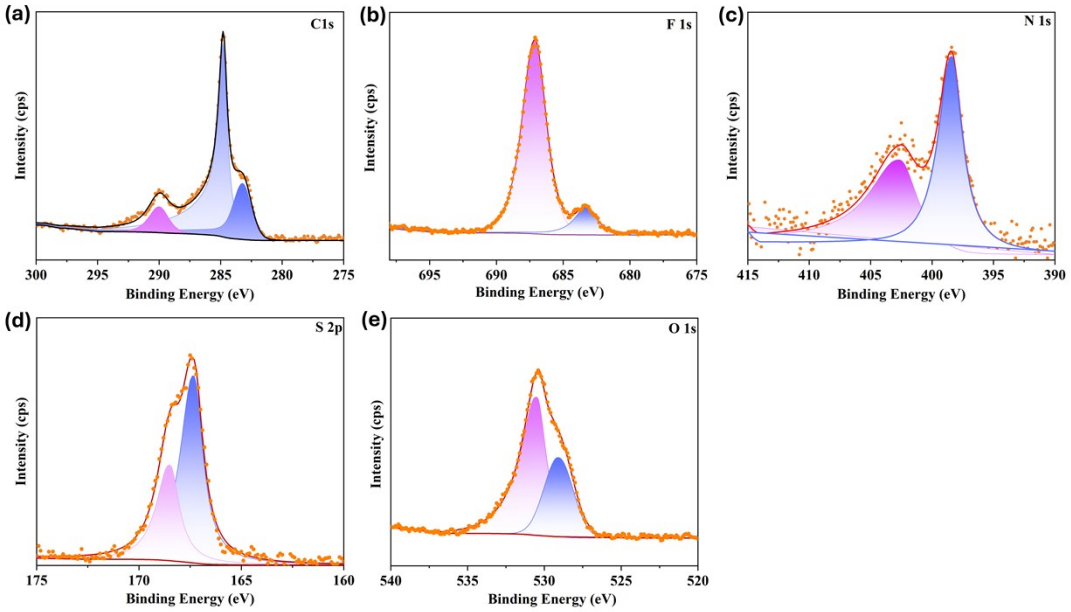

Figure S6. Electrolyte/NCM811 interface XPS analysis of FAN-based heterogeneous LMBs. (a) C 1s spectrum. (b) F 1s spectrum. (c) N 1s spectrum. (d) S 2p spectrum. (e) O 1s spectrum.

Table S1. Porosity and electrolyte uptake of trilayer and PE separators.

Separators	Porosity (%)	Electrolyte uptake (%)
PE	50	40
Trilayer	82	100

Table S2. Fitting parameters of conductivity of the electrolytes versus temperature.

Electrolyte	***A'***	***B*** **(kJ mol^{-1})**	***T_0*** **(K)**	***R^2***	***RMSD***
FAN-TFEA	0.13	2.25	130	0.999	0.00071
FAN-TFEA-5% LLZO	0.12	1.87	135	0.996	0.00379

Table S3. Fitting XPS peak parameters derived by spectra of Li metal anodes after 10 cycles in heterogeneous FAN-based electrolyte.

Spectra	Binding energy (eV)	FWHM (eV)	Atomic percentages (at.%)
C 1s	284.80	1.49	52.6%
	286.86	3.44	25.3%
	290.06	1.61	25.1%
F 1s	684.82	2.14	36.3%
	688.34	2.13	63.7%
N 1s	397.90	1.99	58.8%
	399.43	2.1	41.2%
S 2p	160.62	1.92	37.1%
	161.72	1.92	
	168.63	3.03	62.9%
	169.73	3.03	
O 1s	531.67	2.01	71.4%
	534.37	2.36	28.6%

Li 1s	54.33	1.49	39.8%
	54.92	0.82	18.7%
	55.50	0.66	18.7%
	56.12	0.99	22.7%

All XPS spectral peaks were fitted with AVANTAGE software using Gaussian–Lorentzian line shapes. It fixed the spacing and area ratio of the spin-orbit splitting peaks, constrained the full width at half maximum (FWHM) of multiple peaks belonging to the same chemical state to be identical. The binding energies of all peaks must fall within a reasonable chemical shift range. Shirley backgrounds were used in all fits to narrow scan spectra.

C 1s, F 1s, N 1s, S 2p, O 1s and Li 1s spectral lines consist of a single peak whereas the S 2p spectrum consists of two peaks, a spin-orbit doublet. The S $2p_{1/2}$ peak intensity was assigned precisely half the S $2p_{3/2}$ intensity as required by theory. The two peaks were assigned identical FWHM values. The C 1s spectral line was standardized to 284.8 eV and the F 1s, N 1s, S 2p, O 1s and Li 1s spectra were adjusted to this energy.

Table S4. Fitting XPS peak parameters derived by spectra of Li metal anodes after 10 cycles in single ether-based electrolyte.

Spectra	Binding energy (eV)	FWHM (eV)	Atomic percentages (at.%)
C 1s	284.80	1.16	58.5%
	289.31	2.05	26.9%
	286.60	1.41	14.6%
F 1s	688.92	1.85	85.5%
	684.97	1.68	14.5%
N 1s	399.63	1.66	58.1%
	398.05	2.78	41.9
S 2p	168.95	1.36	33.9%
	170.23	1.36	
	161.88	1.22	23.4%
	162.98	1.22	
	167.13	1.74	28.5%
	168.23	1.74	

	160.21	0.76	14.2%
	161.51	0.76	
O 1s	531.82	1.77	100%
Li 1s	56.09	1.11	22.1%
	55.51	0.89	27.8%
	54.93	0.85	28.3%
	54.33	1.32	21.8%

The S $2p_{1/2}$ peak is separated from the S $2p_{3/2}$ peak by 1.2 ± 0.1 eV.

Table S5. Fitting XPS peak parameters derived by spectra of NCM811 from FAN-based heterogeneous LMBs.

Spectra	Binding energy (eV)	FWHM (eV)	Atomic percentages (at.%)
C 1s	284.80	0.83	65.4%
	289.99	1.49	8.5%
	283.22	1.72	26.1%
F 1s	687.13	2.06	86.2%
	683.33	1.91	13.8%
N 1s	398.42	2.21	55.5%
	402.63	3.45	44.5%
S 2p	167.31	1.07	100%
	168.48	1.07	
O 1s	529.08	2.23	34.2%
	530.48	1.43	65.8%

The S $2p_{1/2}$ peak is separated from the S $2p_{3/2}$ peak by 1.17 eV.

Supporting Note

1 S. Wang, F. Wei, A. R. Polu, P. K. Singh, N. Hu and S. Song, *Small*, 2025, **21**, 2412389.

2 F. Wei, S. Wang, S. V. Savilov, A. R. Polu, P. K. Singh, N. Hu and S. Song, *J. Membr. Sci.*, 2025, **717**, 123590.

3 N.H. Idris, M.M. Rahman, J.-Z. Wang and H.-K. Liu, *J. Power Sources*, 2012, 201, 294.

4 J. Mindemark, M.J. Lacey, T. Bowden and D. Brandell, *Prog. Polym. Sci.*, 2018, 81, 114–143.